ChemCatChem

Research Article
doi.org/10.1002/cctc.202401474

Chemistry Europe
European Chemical Societies Publishing

www.chemcatchem.org

Insights Into Electrocatalytic Hydrogenation of Furfural on Nanoparticulate Pd/C Under Acidic Conditions

Nik Maselj,*[a, b] Vasko Jovanovski,[a] Jan Trputec,[a, b] Martin Šala,[c] Kristina Mervič,[c] Nejc Hodnik,[a] and Primož Jovanovič*[a]

In this work, we present an insight into the mechanism of electrochemical hydrogenation of furfural on carbon supported palladium nanoparticles. By directly coupling electrochemistry with mass spectrometry, we were able to, for the first time, deconvolute the hydrogen evolution reaction and electrochemical hydrogenation by measuring the mass signal for hydrogen and 2-methylfuran. This approach also allowed us to extract the Tafel slopes for each reaction and get insights into mechanisms. The results indicate that the hydrogenation occurs by a Langmuir–Hinshelwood type process rather than by proton-coupled electron transfer. Further findings recognize the blocking character of furfuryl alcohol (FA) where the latter or one of its intermediates blocks the electrochemical hydrogenation. Additionally, FA is shown to be a precursor for 2-methyl furan formation. Accordingly, specific guidelines towards improvement of reaction performance are suggested.

1. Introduction

Aldehyde reductions are needed to convert biomass into value-added chemicals such as, fuels and monomers. Furyl aldehydes, such as furfural (FF) and 5-hydroxymethylfuran (HMF), are molecules of great importance as platform chemicals that are usually obtained through the acid-catalyzed removal of water from pentoses and hexoses. These molecules have a similar structure, consisting of a furan ring with an aldehyde functional group (—C═O). Selective reduction of these oxygen-containing moieties is crucial for the production of valuable platform molecules that are used en route to important chemicals. Key examples include furfuryl alcohol (FA, a precursor for polymers), 2-methylfuran (2-MF, employed as a drop-in jet fuel) and 2,5-bis(hydroxymethyl)furan (used as a precursor for resins and chemicals). However, the chemical upgrading of furyl aldehydes from biomass often requires high pressures and temperatures as well as large amounts of externally supplied hydrogen. In this respect, electrochemical hydrogenation and hydrogenolysis (ECH) of biomass fueled by renewable electricity under ambient conditions can be an alternative. Accordingly, research efforts in this field have intensified in recent years, with a particular focus on the electrochemical hydrogenation of biomass due to the higher techno-economic interest of FF (annual production capacity of more than 2 million tons).[1–3] However, if electrochemical routes for the valorization of biomass-derived FF are to be established as a credible alternative, a systematic development of ECH catalysts and concomitant understanding of the reaction mechanism is a necessity. As far as the ideal catalyst is concerned, the (experimentally determined) ECH rates of aldehydes, including FF, and the corresponding (theoretically calculated) binding energies follow the Sabatier principle (volcano-like plot).[4] Accordingly, in the case of benzaldehyde and FF, Pd sits at the top of the volcano curve. The derived rate expressions consider two mechanisms, a Langmuir–Hinshelwood (L–H) and proton-coupled electron transfer (PCET), however regardless of the specifics, hydrogenation occurs as an inner-sphere hydrogen addition or electron transfer.[5–8] Two possible scenarios are considered, namely a regime with high H_{ads} (θ_H) or high aldehyde coverage regime (θ_{RCHO}), respectively. The corresponding rate equations could not differentiate between the L–H and PCET mechanisms for the case of a high H_{ads} regime. In contrast, under a high θ_{RCHO} regime, the ECH reaction can follow either the L–H or PCET path. Overall, the conclusions indicate that different ECH mechanisms and reaction regimes are at play for different type of metals.[4] Indeed, several research groups have shown that surface hydrogenation via H_{ads} plays only a minor role in ECH compared to the proton-coupled electron transfer (PCET) steps.[9,10] This trend was ascribed to the negligible H_{ads} coverage (in the case of Cu and FF) under ECH conditions and the high activation barriers for surface hydrogenation.[9] Regardless, the ECH performance of aldehydes is controlled by the interplay between hydrogen and the aldehyde molecule for active sites on

[a] N. Maselj, V. Jovanovski, J. Trputec, N. Hodnik, P. Jovanovič
Department of Materials Chemistry, National Institute of Chemistry, Hajdrihova 19, Ljubljana1000, Slovenia
E-mail: nik.maselj@ki.si
primoz.jovanovic@ki.si

[b] N. Maselj, J. Trputec
Faculty of Chemistry and Chemical Engineering, University of Ljubljana, Večna pot 113, Ljubljana1000, Slovenia

[c] M. Šala, K. Mervič
Department of Analytical Chemistry, National Institute of Chemistry, Hajdrihova 19, Ljubljana1000, Slovenia

Supporting information for this article is available on the WWW under https://doi.org/10.1002/cctc.202401474

the surface. This emphasizes the need for a harmonious relationship between the binding energies of aldehyde and hydrogen to facilitate ECH. In other words: If the hydrogen binding energy is too high, the binding energy of the aldehyde must be sufficiently high for it to be adsorbed on the metal surface. However, if the aldehyde binding energy is too high, it can deactivate the ECH.[4,11]

Herein we investigate the performance of commercially available nanocomposite palladium nanoparticles on high surfaces area carbon support (Pd/C) towards FF reduction under acidic conditions, using a unique diagnostic, namely electrochemistry coupled with mass spectrometry (EC–MS). This particular choice is justified by practical relevance, where the acidic Nafion membrane is used in proton exchange membrane (PEM) reactors. Hence, the conditions within the membrane electrode assembly (MEA) and the uncontrolled oscillation of the potential in the region of base metal instability impose restrictions on the choice of metal catalysts suitable for hydrogenation to protect them from degradation. To date, only Cu electrodes have demonstrated the unique ability to form hydrogenolysis products with high selectivity[9] (i.e., 2-MF, a compound of greater economic importance than FA).[12–14] Therefore, the field would benefit from a better understanding of ECH processes on electrochemically more noble and thus stable metals such as Pd.

2. Experimental Section

2.1. Voltammetry Under Stagnant Regime

A commercial nanoparticulate catalyst 20 wt % Pd on carbon was investigated (Premetek). A detailed structural characterization of the sample can be found in our recent publication. Briefly, according to transmission electron microscopy (TEM) imaging Pd/C sample contains uniform-sized Pd nanoparticles, the majority of which have a diameter in the range between 2 and 6 nm.[15] Electrochemical experiments were performed in a single-compartment glass cell using the glassy carbon disc (GC, $d = 3$ mm) as the working electrode (WE), Basi), a reversible hydrogen electrode (RHE, Gaskatel HydroFlex) as the reference electrode (RE) and graphite rod as the counter electrode (CE). The GC electrode was polished on a 0.5 µm polishing slurry on a Trident Polishing Cloth (Buehler, USA) prior to the application of the catalyst suspension. Before being applied to the GC electrodes the suspensions were sonicated for 20 min. For a description of the catalyst suspensions see section electrochemistry coupled with mass spectrometry. All experiments were performed in 0.1 M $HClO_4$ (prepared from 70% Rotipuran® Supra $HClO_4$, Carl Roth), and variable concentrations of FF (Sigma–Aldrich). All electrochemical measurements were performed using a Biologic SP-300 potentiostat.

2.2. Rotating Disc Electrode Voltammetry

Experiments were carried out using a GC rotating disc electrode (Pine, $d = 5$ mm, RDE) in a standard three compartment cell. The RE used was a RHE (Gaskatel HydroFlex), and a graphite rod as the CE. Before applying the Pd/C ink to the GC the same procedure as in other electrochemical measurements was performed.

2.3. Electrochemistry Coupled with Mass Spectrometry

EC–MS experiments were performed with the Spectro Inlets EC–MS system. The make-up gas used in measurements was 5.0 Helium (Messer). After each measurement, a calibration of the MS detector was performed. The calibration protocol for H2 comprised a sequence of galvanostatic pulses (75, 50, 40, 30, 20, 10, 5 µA), 2 min each, where a polycrystalline platinum disc (Pine, $d = 5$ mm) was used as the WE. The RE used was a RHE (Gaskatel HydroFlex), and a coiled Pt wire was used as the CE. In between pulses, a rest period of 10 min under controlled potential (0.1 V vs. RHE) was imposed to ensure the MS signal for hydrogen returned to baseline. Afterwards, a calibration curve was made by comparing the electrochemical charge obtained from the pulse with the integrated area of the MS signal for hydrogen. A separate calibration was also performed in which a gas mixture containing 1% hydrogen in argon was used as a makeup gas. ECH experiments were performed in 50 mM FF (Sigma–Aldrich) in 0.1 M $HClO_4$ using potentiostatic pulses. These were chosen in the range between 0.2 V and −0.35 V (vs. RHE), or as negative as possible keeping in mind the limit of the setup (more than 100 µA of constant H_2 production results in bubbles that significantly interfere with the measurement).[16,17] Pulses lasted for 2 min with a rest period after each pulse to ensure the monitored MS signals returned to the baseline. In the case of 2-MF quantification, the same calibration protocol as described in detail in our recent publication was followed.[18] Catalyst films were prepared by drop-casting 10 µL of freshly sonicated catalyst suspension onto a GC disc ($d = 5$ mm). The disc was left to dry completely before use. The catalyst suspensions used were prepared by adding 5 mg of Pd/C (Premetek, 20%) to 3 mL of solvent (75% Isopropanol, 25% ultrapure water). After a brief sonication 65 µL of 5 wt% Nafion® solution was added and suspension was sonicated. The suspension used in lower loading experiments was prepared by preparing a suspension of 2.28 mg of Pd/C in 1.368 mL water with added 0.465 mL isopropanol and 24.64 µL of 5 wt% Nafion® solution. 0.5 mL of this solution was then diluted to 5 mL by adding 3.36 mL of water and 1.14 µL of isopropanol. The mass of Pd on the electrode in the high loading case is 3.2 µg and 0.33 µg in the low loading case.

2.4. Electrochemical Flow Cell Experiment

A custom-made electrochemical cell flow was used for experiments where FA was pursued as the product. The cell encompassed a GC disk ($d = 5$ mm) as WE. The RE and the CE were separated from the working compartment by glass frits (see Figure S2). The flow of electrolyte was established using a syringe pump with a flow rate of 20 mL/h. The electrolyte used was 50 mM FF in 0.1 M $HClO_4$ (prepared from 70% Rotipuran® Supra $HClO_4$, Carl Roth).

2.5. HPLC Analysis

HPLC-UV–Vis analysis was performed on Ultimate 3000 UHPLC system (Thermo Scientific, U.S.A.). Methanol (Chromasolv LC-MS grade, Fluka, Switzerland) and water purified on a Milli-Q system from Millipore (Bedford, MA, USA) were used for the preparation of mobile phases, formic acid from Fluka (p.a. grade purity) was used as modifier. An analytical EC HPLC column Nucleodur C18 HTec (2.0 × 150 mm, 3 µm particle size, Macherey–Nagel) was used with the flow rate of 0.3 mL min^{-1} (the details on method gradient are given in Supporting Information, (Section S2). A mobile phase consisting of acetonitrile and water, both with 0.1% formic acid, was used throughout the work. Injection volume and column temperature were 10 µL and 30 °C, respectively.

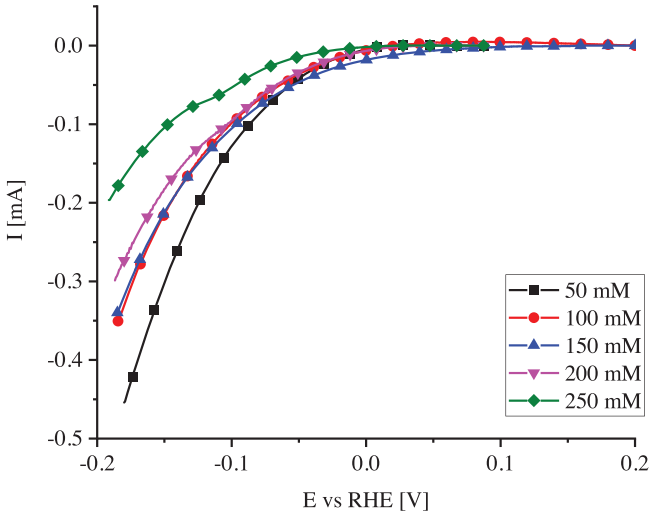

Figure 1. Comparison of voltametric responses of Pd/C under increasing concentrations of FF in 0.1 M $HClO_4$.

3. Results and Discussion

Our initial experiments targeted at voltametric response of stationary nanoparticulate Pd/C electrode under ECH potentials. We emphasize that understanding voltammetry under the stationary regime is particularly important due to the relevance of electrochemistry and mass spectrometry coupling for product analysis (the EC–MS technique) employed in the subsequent step. Namely, due to the setup limitations electrochemical experiments in the EC–MS configuration can only be performed under a stagnant regime. The goal therefore was to elucidate if the current response under ECH potentials is subjected to mass transport limitations. For this purpose, voltametric response under gradually increased FF concentration (50-250 mM) was monitored. The current decreased when the concentration of FF increased suggesting that the FF reduction (at this point hypothesized as the predominant reaction) is kinetically controlled (Figure 1).

To confirm that the Faradaic response is indeed ascribed to the ECH reaction solely, experiments with the EC–MS apparatus were performed. This enabled the detection of volatile compounds from the electrode surface with high sensitivity in close to real-time. In particular, we focused on pursuing 2-MF and H_2 from competitive hydrogen evolution reaction (HER). According to the EC–MS analysis, the two compounds are clearly detected under potentiostatic biasing (Figure 2a,b). ECH is the dominant reaction above -0.3 V versus RHE and is near zero order with respect to FF concentration (Figure 1). ECH dominance is directly confirmed by 2-MF occurrence which can be detected from 0.1 V onwards cathodically (Figure 2b,c). As shown in continuation the residual part of the Faradaic charge is contributed by the FA formation, the other possible ECH product under these particular conditions.[3,19–21] Note however, FA cannot be monitored via EC-MS diagnostics due to its insufficient volatility (according to Henry's law solubility constant $H^{cp}{}_s$ values 15,000 times less volatile as 2-MF at 25 °C).[22] Note that, for adequate EC–MS detection the analyte needs to first diffuse from the WE to the chip, and subsequently change from solution to the gas phase in the membrane chip. However, the low volatility of FA prevents direct MS detection. Instead, FA was quantified via HPLC analytics.

For this purpose, a custom built electrochemical flow-type cell was used in which the downstream electrolyte was collected and subsequently analyzed using HPLC diagnostics. Of the products, only FA was detected. The concentration of 2-MF was below the detection limit. Nevertheless, the combination of HPLC and EC–MS results undoubtedly confirms that Pd is highly selective towards the FA product under the chosen electrochemical conditions. This is rather expected considering the analogy with benzaldehyde reduction.[23–28]

The combined results of voltammetry, EC–MS and HPLC analysis provide some important insights into the mechanism of FF reduction. Although FF reduction dominates compared to HER within the entire potential range, some H_2 can be clearly identified via EC–MS diagnostics (Figure 2). This strongly implies the dominance of H_{ads} involving pathways[11,19,20,29–32] in Pd-based ECH instead of the PCET one. Note that, if the hydrogenation of FF indeed occurs via PCET (as has recently been reported for the low H coverage metals, e.g., Cu[9]) then one would not expect HER to proceed simultaneously with ECH. Furthermore, our results imply that HER and ECH reactions compete for the same active sites since the addition of FF decreases the current that passes through the cell at low overpotentials compared to 0.1 M $HClO_4$. Interestingly, this contrasts with the analogue of benzaldehyde (BA) ECH where an Eley–Rideal mechanism (E–R) was proposed to operate via PCET steps. However, we emphasize that in the latter case, one could not distinguish between the E–R and the L–H mechanism and the E–R path was presumed due to the seemingly complete HER inhibition.[24] Note that this observation could solely be due to the insufficient sensitivity of gas chromatography coupled with a thermal conductivity detector towards H_2 detection. On the contrary, in the present study, the extremely sensitive EC–MS analysis is crucial. We still allow the possibility that direct comparison between BA and FF ECH is not credible as the two analogues might follow a different mechanism considering they adsorb in a different configuration, that is, via tilted geometry with the –CHO group (FF case) or via a flat geometry with the ring (BA case).[33–38] Our further analysis focused on the extraction of Tafel slopes for the ECH. As far as we know, this is the first time that accurate Tafel slopes for HER in the FF presence, and the two ECH products have been obtained for Pd case. Again, it should be noted that a meaningful Tafel analysis is possible due to the absence of mass transport limitations (Figure 1) and because the unique EC-MS diagnostics allows the partial current densities to be decoupled for each reaction based on calculating the Faradaic current from the MS signal. That is, for each potential pulse the average current was divided by the faradaic efficiency obtained from the MS signal, yielding the average current for each reaction product. Accordingly, a single slope of 118 mV/dec is obtained for HER (Figure 3a) analogously to FF-free HER[39–41] indicating the initial hydrogen adsorption (Volmer step) is the rate determining step.[42] For ECH, a single Tafel slope of 96 mV/dec is obtained for 2-MF formation, whereas

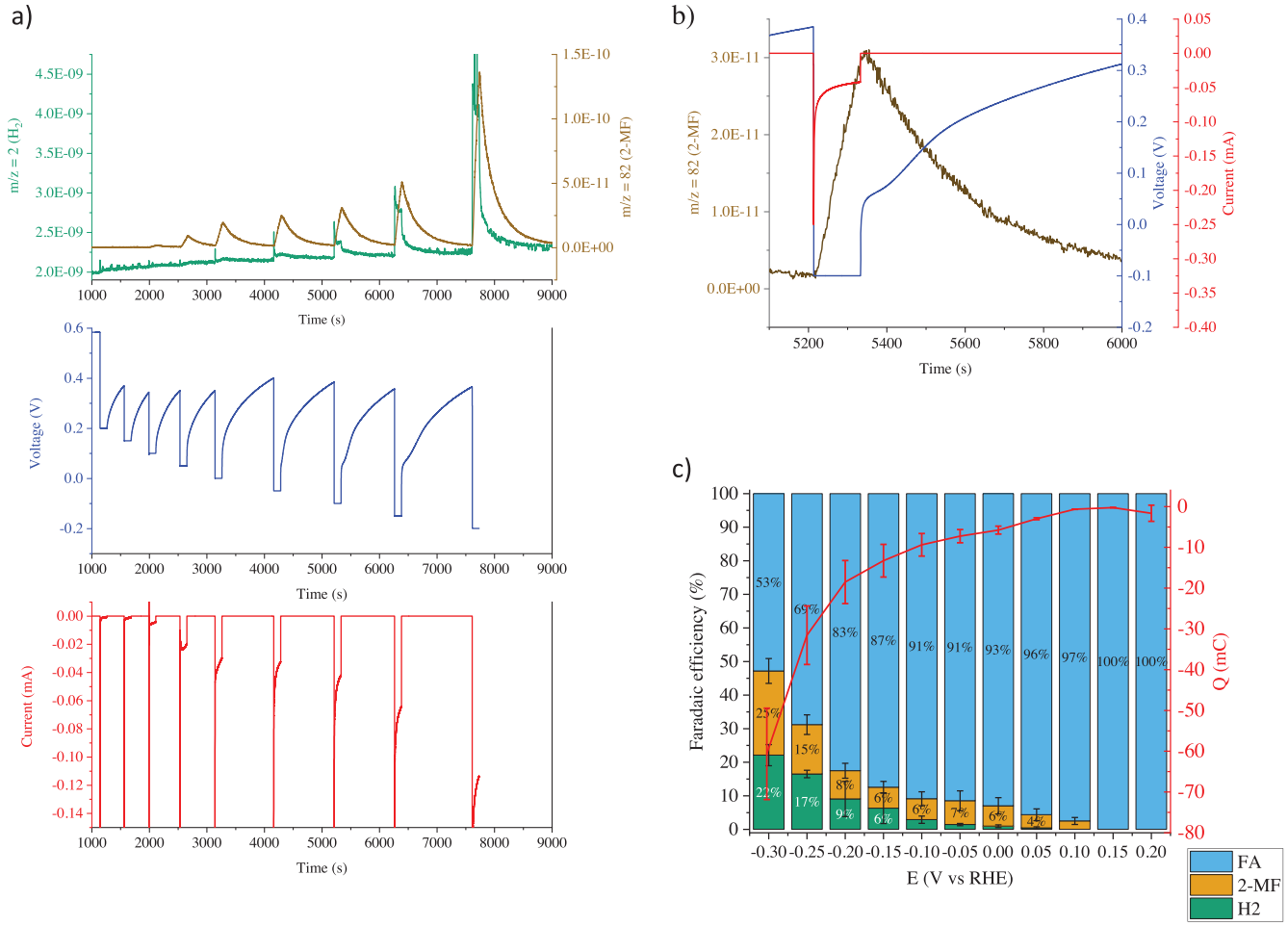

Figure 2. (a) EC–MS data showing potentiostatic pulses and corresponding increases in measured mass signals (current from the electron multiplier) for Hydrogen (m/z = 2, green line) and 2-MF (m/z = 82, amber line) in a 50 mM FF / 0.1 M $HClO_4$ solution. (b) A close up of EC–MS data showing the signal for 2-MF increase and continuing to increase for the duration of the potentiostatic pulse. (c) Faradaic efficiencies at each potential for HER and ECH reaction obtained from the separately prepared calibration curves.

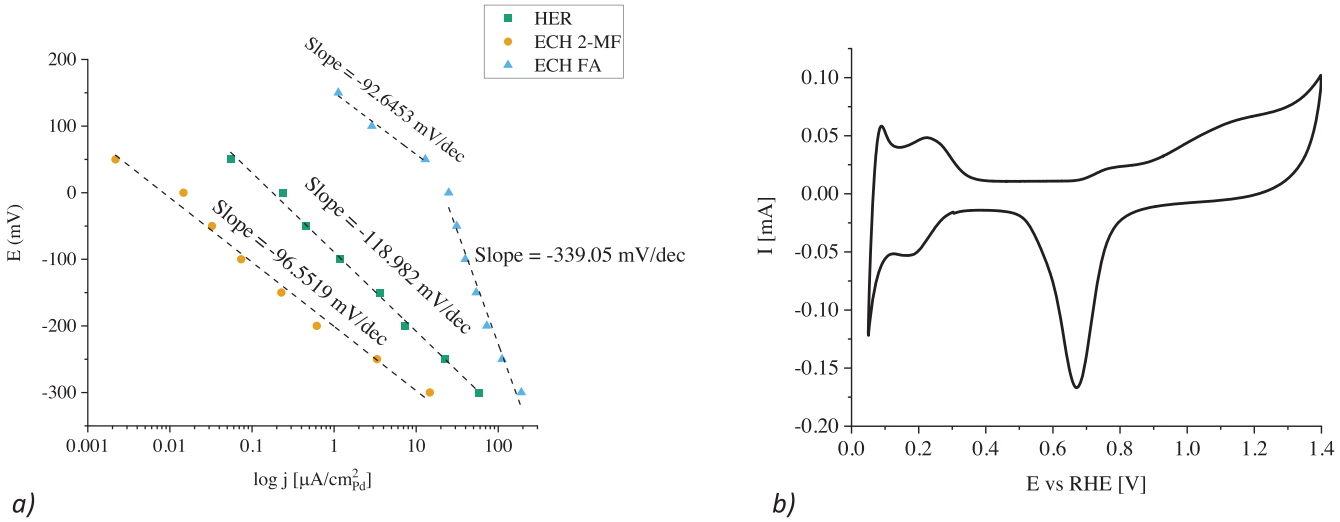

Figure 3. (a)Tafel slope for HER, and both ECH reactions decoupled using EC–MS. The partial currents for each reaction were obtained by multiplying the total current density with the faradaic efficiencies for each reaction. (b) Cyclic voltammogram (@ 50 mV/s) of Pd/C in 0.1 M $HClO_4$.

for the FA, the slope is potential dependent. Namely, a value of 93 mV/dec is retrieved at low overpotentials and a value of 339 mV/dec at high overpotentials (Figure 3a). The value at low overpotentials shows that the first H_{ads} addition is the RDS for both ECH products. Theoretically a value of 120 mV/dec is expected, whereas if the second H_{ads} addition were the RDS, one would expect a Tafel slope on the order of ~ 40 mV/dec, as is the case of copper surfaces.[9] Several factors could cause the discrepancy with the theoretical values, e.g. variations in the transfer coefficient,[43] potential dependent surface coverage,[42] changes in the effective surface area[44] during the reaction or mass transport limitations.[45] However, as demonstrated above, the latter do not appear to be present, as manifested in voltametric response at different FF concentrations (Figure 1). On the other hand, the increase in Tafel slope for FA formation at lower potentials (339 mV/dec, Figure 3a) implies that the ECH process eventually becomes susceptible to the formation of palladium hydrides via H absorption into the crystal lattice and formation of α and β hydrides (PdH_x)[41,46–49] and/or increased coverage of adsorbed reaction intermediates/products.[42] We note that this assumption is only valid if the reaction indeed proceeds via a PCET mechanism. As for PdH_x, its formation closely overlaps with the transition of the slopes to higher values (Figure 3a,b) emphasizing that the Faradaic contribution of FA formation cannot be accurately decoupled via EC-MS analysis. Note that H absorption typically proceeds below 0.1 V.[41,47,48,50] However, in the presence of strongly adsorbing FF, this window likely shifts to more cathodic potentials. More accurate decoupling of the contribution of FA formation Faradaic response is possible within the flow cell (i.e., controlled mass transport) in conjunction with downstream HPLC analysis of FA where a Tafel slope of ≈ 200 mV/dec is obtained from HPLC analysis (Figure S3). Considering that this value is still somehow larger than the theoretically derived value (≈ 120 mV/dec), it can be reasonably assumed that the adsorbed reaction intermediates/products manifest an inhibitory role for ECH. This hypothesis was pursued in continuation by employing an RDE configuration.

Overall, much better performance is obtained under hydrodynamic regime (Figure 4a), together with a Tafel slope of 120 mV/dec (Figure S3), which is a theoretically expected value for FA formation and much lower than the value obtained under the stagnant regime (339 mV/dec, Figure 3a). Accordingly, one can hypothesize that the polarization curves are strongly susceptible to surface-blocking phenomena. To substantiate this further, potentiodynamic experiments were performed in which the scan speed was varied, which led to an additional improvement of ECH performance (Figure 4a) as is discussed later. Overall, this suggests a time dependence of the ECH, where longer exposure to reaction leads to worse performance implying that the accumulated ECH intermediates and/or products have a blocking character. As for the products, the adsorption of the dominant product, that is, FA, could block the surface and inhibit further reaction. In regard to the ECH intermediates potential candidates are either FCH_2O^* or FCHOH* formed via the first H_{ads} addition (FA formation path) and/or FCH_x^* intermediates ($x = 1, 2, 3$) formed in the subsequent H_{ads} additions (2-MF formation path, see Figure S1). Considering that FA is the predominant ECH product (several times higher current densities than in the 2-MF case, see Figure 3a), it is reasonable to assume that either FCH_2O^* or FCHOH* are the predominant blocking species. This might indeed be the case if we assume the copper case, where in particular the high coverage of FCHOH intermediate was demonstrated to inhibit ECH.[9] Note that the same effect could explain the deviations from theoretical Tafel slope (Figure 3a). We addressed the FA scenario by performing separate voltametric experiments to monitor HER (FF-free solution) either under FA-free conditions or under different FA concentrations. Accordingly, the polarisation under the FA-free conditions significantly differs from the FA analogues (Figure 4b), strongly suggesting the blocking nature of FA. A similar effect was observed in heterogeneous catalysis where FA desorption was found to be the limiting factor for FF hydrogenation.[51,52] Note, however, that this does not exclude the potentially inhibitory role of ECH intermediates at this point. Interestingly though, the FA induced inhibition of HER is in stark contrast to the copper analogy, in which HER is not inhibited.[10,19]

To pursue the characteristics of time dependence further, we performed voltametric experiments under ECH potentials by varying the scan rate. Such trends could provide further evidence of the blocking effect, as the surface coverage of ECH intermediates/products could be proportional to the scan rate, as has been shown in other reactions.[53–56] That is, the longer the accumulation time, the more intermediates/products can be adsorbed on the surface and thus block the reaction. According to the voltammograms obtained, the current response indeed increases gradually with the scan rate (Figure 4a), supporting the hypothesis of the blocking nature of the ECH intermediates/products. Further evidence for the blocking effect of ECH intermediates/products was obtained by combining electrochemical performance data with either in-situ or downstream product analysis. For this purpose, either electrochemical flow with subsequent HPLC analytics (FA quantification) or EC-MS analysis (2-MF quantification) were employed. First, a comparative analysis of two test series was carried out, which differed in the chronoamperometric sequence. The chronoamperometric treatment was carried out either by gradually decreasing the potential from 0 V in the cathodic direction in steps of 100 mV or in steps of 50 mV. The purpose of such comparison is to inspect whether or not electrochemical exposure to ECH proceeding has any effect on product formation (FA in this case). We note that the same catalyst loading was used for both experiments, which is an important parameter as will be shown in continuation. The results show a strong effect of the increment step, where the 100 mV analogue performs significantly better than the 50 mV case (Figure 5a,b) in line with the trends from the scan rate experiment (Figure 4a).

Additional experiments were performed with different catalyst loadings aiming to distinguish between the role of ECH intermediates and products (i.e., FA). More specifically, if adsorbed intermediates play a central role in ECH inhibition, then in theory, the ECH selectivity (i.e., FE) should not change with a change in the catalyst loading (if there are no mass transport limitations, as indeed is the case as shown above). Note that the potential intermediates discussed here (FCH_2O^* or FCHOH*) are only con-

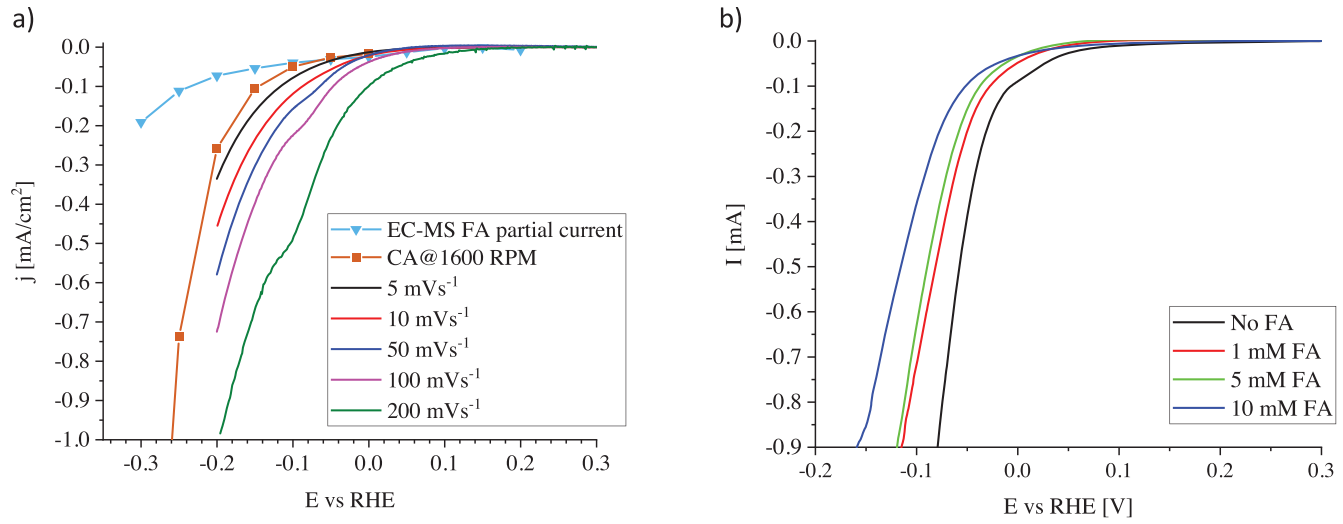

Figure 4. (a) Comparison of LSV polarisation curves under different scan rates alongside reconstructed LSV from potential steps in RDE and EC–MS extracted partial current densities for FA. CA denotes that a chronoamperometric biasing was employed. (b) CVs in the presence of increasing concentrations of FA.

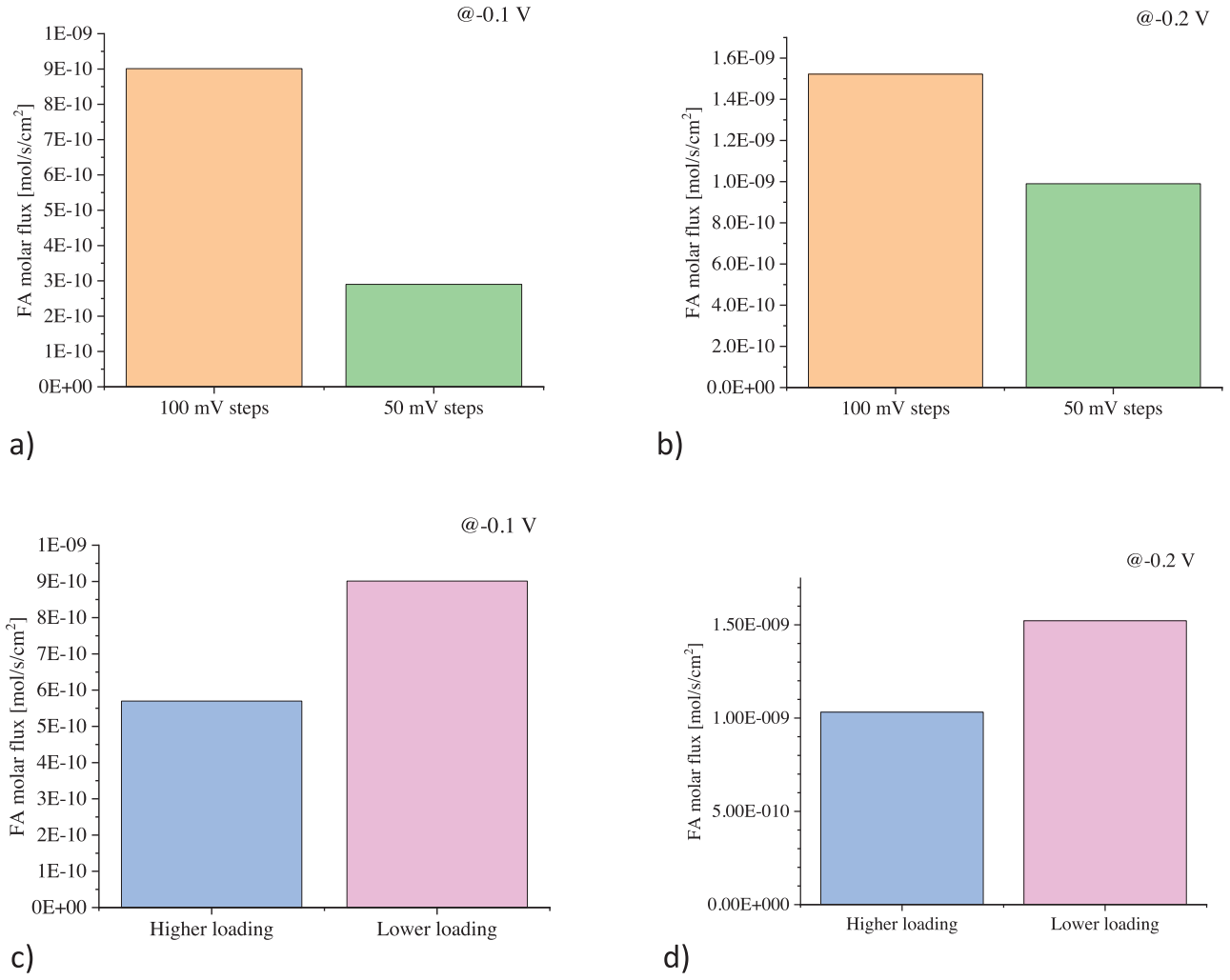

Figure 5. FA molar flux calculated from HPLC product quantification. (a,c) at −0.1 V and (b,d) at −0.2 V. The Pd loading in the higher loading case is 3.2 μg and in the lower loading case is 0.33 μg of Pd. The surface areas are 1.91 cm^{-2} and 0.14 cm^{-2} respectively.

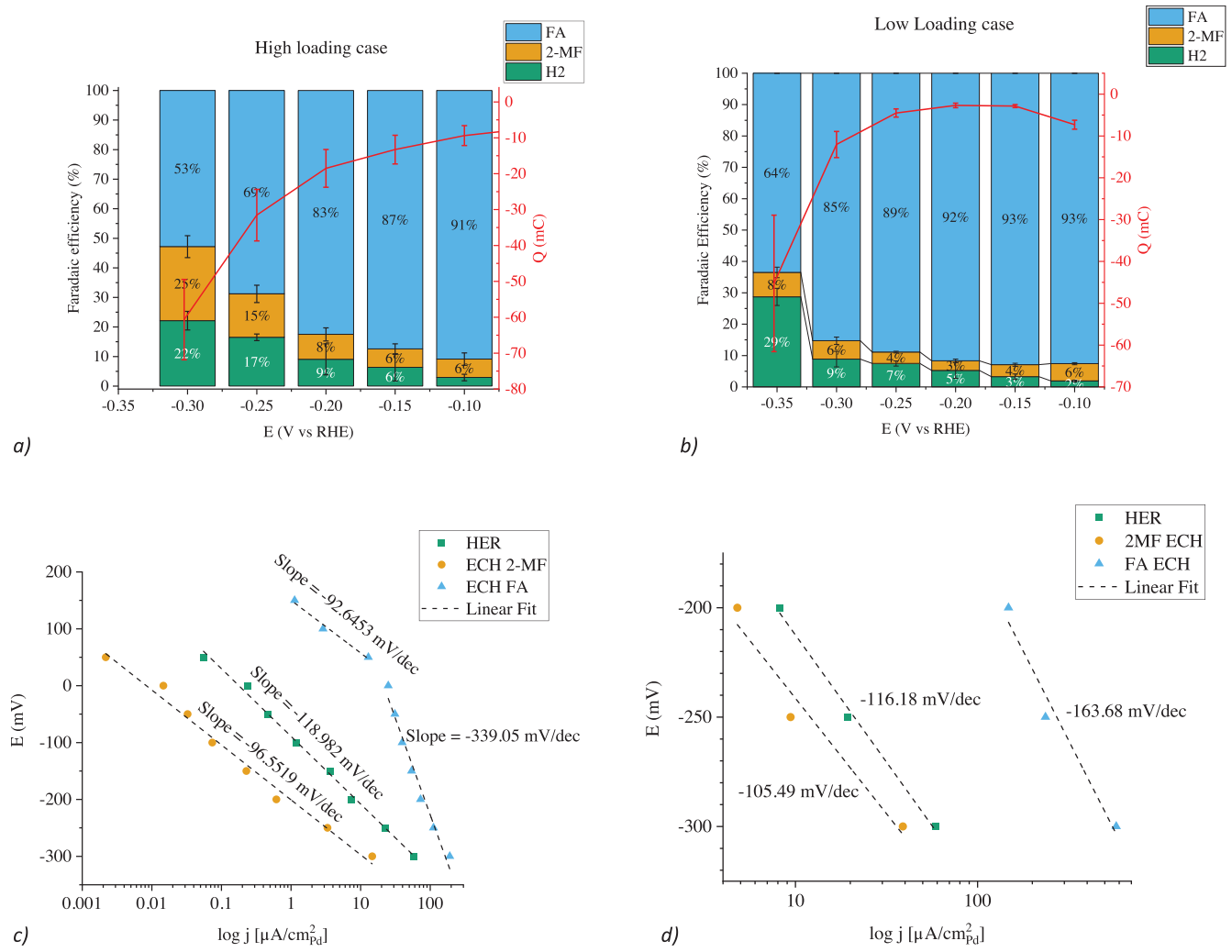

Figure 6. (a) High loading/same as in Figure 4a., (b) Low loading case. (c) and (d) Decoupled current densities as Tafel curves for high loading and low loading respectively.

sidered as adsorbed species. On the other hand, if FA plays the predominant inhibitory role as the main product, the reaction selectivity could potentially change. Namely, the surface coverage of FA is directly proportional to its concentration within the catalyst film and potential (i.e., adsorption isotherm) where with an increase in the film thickness the concentration of FA within the film increases. Indeed, in the case of FA, the amount normalized per Pd surface area decreases with increasing loading of the catalyst (at higher loading case the loading of the catalyst is twice as high as in the low loading case), confirming the inhibitory role of FA (Figure 5c,d). An analogous experiment coupled with an EC–MS analysis was performed to monitor 2-MF and H_2 for the case of two different Pt/C loadings. The observed trend indicates that catalyst loading has a significant effect on the production of 2-MF and H_2. In particular, increasing the loading leads to a several-fold increase in the faradaic efficiencies of H_2 and 2-MF across the entire potential range (Figure 6a,b). Furthermore, based on the decoupled partial current densities, there is a lower slope for FA production in the lower loading case (≈ 160 mV/dec), approaching the theoretically expected value of 120 mV/dec. Note that the slopes for 2-MF and H_2 formation do not change significantly. However, the 2-MF specific current density (reaction rate) increases by about 8 times when the loading is decreased (at −0.2 V, Figure 6c,d). Overall, the trends obtained give further credence to the blocking character of FA which inhibits the formation of both ECH products.

Overall, the combined HPLC and EC-MS trends show a strong dependence of the ECH selectivity and the formation rates of the products on the catalyst loading. In particular, increasing the loading increases the selectivity towards 2-MF while decreasing the formation rate, as seen from the current densities in the Tafel slopes (Figure 6c,d), which raises important questions about the ECH pathway on the Pd surface and the role of FA. More specifically, the increased selectivity towards 2-MF appears to be related to the increasing coverage by FA, suggesting that FA is a precursor for 2-MF. Note that this would be in contrast to the Cu case.[9,10,29,32] To elucidate this, we performed electrochemical experiments in the FA solution (FF-free solution) via the EC-MS diagnostics. Indeed, a well-resolved MS signal for 2-MF was obtained (Figure 7) confirming the hypothesis on the precursor

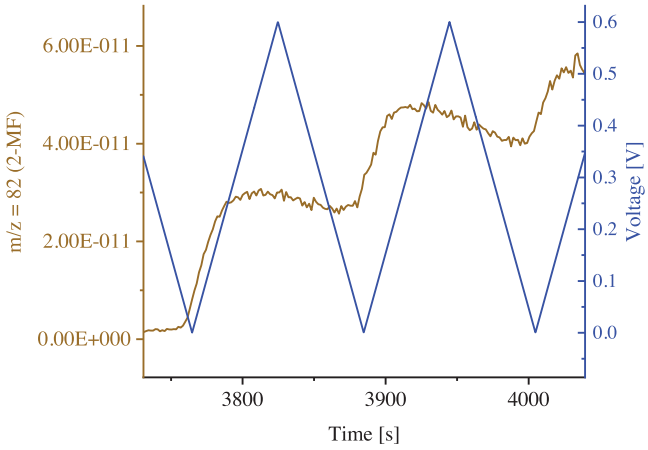

Figure 7. EC–MS monitoring of 2-MF signal during cyclic voltammetry (@10 mV/s) in 25 mM FA in 0.1 M $HClO_4$.

role of FA. On the other hand, the 2-MF formation rate decreases with increasing FA coverage. This is consistent with the results of the Tafel analysis that the first hydrogenation step is the RDS, which requires free Pd sites for H_{ads}. We hypothesize that FCHOH* is formed in the initial step given the barriers for protonation of O and C on metal surfaces[57] and the recent study demonstrating kinetic favorability over the FCH_2O* analogue.[9] With respect to HER, the trend obtained suggests that as FA coverage increases by increasing catalyst loading, the coverage of H_{ads} also increases, which translates into increased selectivity towards H_2 in the entire potential range. This trend also indicates that FA causes repulsive interactions with FF, resulting in more vacancies for H_{ads}. Unlike the formation of FA and 2-MF, HER kinetics remain virtually unchanged (at −0.2 V, Figure 6c,d) when loading is changed, suggesting that increased coverage with FA does not alter H-binding energy.

4. Conclusions

The results presented herein open up a plethora of possibilities for the systematic engineering of ECH catalysts. In particular, first we show that the ECH of FF on the Pd surface is likely governed by a H_{ads} addition and not by the PCET and that the first H_{ads} addition appears to be the RDS. Secondly, ECH is susceptible to adsorption of FA product that inhibits the reaction and alters the selectivity. The mechanistic findings can now be used in particular for more selective 2-MF production (i.e., a more economically valuable product). Here, it would be of considerable importance if the H_{ads} addition pathway could be replaced by a PCET pathway, as the latter would enable more manipulation with the polarizability of the carbonyl group.[58] In this way, the required energy for H^+ to approach the carbonyl group can be decreased, which can be achieved in several ways. One possibility is the use of co-adsorbates with, for example, a hydroxyl group that acts as a proton conduit by forming a hydrogen bond with the carbonyl group.[35] As has been shown in molecular electrocatalysis, such hydrogen-bonded complexes allow for energetically more favorable hydrogen addition.[59,60] Therefore, changing the acid strength of the co-adsorbate (pK_a) seems to be one of the reasonable measures to further improve ECH performance when PCET mechanism is in play.[61]

Additionally, the FA effect gives strong incentive to operate the ECH with a pulsed-bias electrochemical protocol. By alternating the electrode between cathodic and anodic potentials, one could selectively remove adsorbed FA under anodic bias while operating ECH under cathodic biasing. Note that such a strategy has already been used in the electrochemical reduction of CO_2 to suppress the competitive HER.[62–69]

Acknowledgements

This study was supported by the Slovenian Research Agency for the research programs P2–0393 and I0–0003, and projects J1–4401, N1-0224, N2–0248, N2–0155, and MN-0007–104.

Conflict of Interests

The authors declare no conflict of interest.

Data Availability Statement

The data that support the findings of this study are available from the corresponding author upon reasonable request.

Keywords: Electrocatalysis · Electrochemical hydrogenation · Electrochemistry–mass spectrometry · Furfural

[1] R. Mariscal, P. Maireles-Torres, M. Ojeda, I. Sádaba, M. L. Granados, *Energy Environ. Sci.* **2016**, *9*, 1144–1189.
[2] B. R. Caes, R. E. Teixeira, K. G. Knapp, R. T. Raines, *ACS Sustainable Chem. Eng.* **2015**, *3*, 2591–2605.
[3] Y. Kwon, K. J. P. Schouten, J. C. Van Der Waal, E. De Jong, M. T. M. Koper, *ACS Catal.* **2016**, *6*, 6704–6717.
[4] J. A. Lopez-Ruiz, E. Andrews, S. A. Akhade, M.-S. Lee, K. Koh, U. Sanyal, S. F. Yuk, A. J. Karkamkar, M. A. Derewinski, J. Holladay, V.-A. Glezakou, R. Rousseau, O. Y. Gutiérrez, J. D. Holladay, *ACS Catal.* **2019**, *9*, 9964–9972.
[5] Y. Song, S. H. Chia, U. Sanyal, O. Y. Gutiérrez, J. A. Lercher, *J. Catal.* **2016**, *344*, 263–272.
[6] C. Zhao, J. He, A. A. Lemonidou, X. Li, J. A. Lercher, *J. Catal.* **2011**, *280*, 8–16.
[7] J. He, C. Zhao, J. A. Lercher, *J. Am. Chem. Soc.* **2012**, *134*, 20768–20775.
[8] M. Wang, H. Shi, D. M. Camaioni, J. A. Lercher, *Angew. Chem., Int. Ed.* **2017**, *56*, 2110–2114.
[9] S. Liu, Z. Mukadam, S. B. Scott, S. Ch Sarma, M.-M. Titirici, c. K. Chan, N. Govindarajan, a. E. I. L. Stephens, G. Kastlunger, *EES Catal* **2023**, *1*, 539–551.
[10] L. Zhou, Y. Li, Y. Lu, S. Wang, Y. Zou, *Chinese J. Catal.* **2022**, *43*, 3142–3153.
[11] H. Liu, D. M. Patel, Y. Chen, J. Lee, T. H. Lee, S. D. Cady, E. W. Cochran, L. T. Roling, W. Li, *ACS Catal.* **2022**, *12*, 14072–14085.
[12] J. P. Lange, E. Van Der Heide, J. Van Buijtenen, R. Price, *ChemSusChem* **2012**, *5*, 150–166.
[13] K. Yan, G. Wu, T. Lafleur, C. Jarvis, *Renew. Sustain. Energy Rev.* **2014**, *38*, 663–676.
[14] A. Bohre, S. Dutta, B. Saha, M. M. Abu-Omar, *ACS Sustain. Chem. Eng.* **2015**, *3*, 1263–1277.

[15] M. Smiljanić, M. Bele, L. Moriau, F. Ruiz-Zepeda, M. Šala, N. Hodnik, *J. Phys. Chem. C* **2021**, *125*, 27534–27542.
[16] D. B. Trimarco, **2017**.
[17] S. B. Scott, Isotope-Labeling Studies in Electrocatalysis for Renewable Energy Conversion, and the Net Carbon Impact of This PhD Project, **2019**.
[18] N. Maselj, V. Jovanovski, F. Ruiz-Zepeda, M. Finšgar, T. Klemenčič, J. Trputec, A. R. Kamšek, M. Bele, N. Hodnik, P. Jovanovič, *Energy Technol.* **2023**, *11*, 2201467, https://doi.org/10.1002/ente.202201467.
[19] X. H. Chadderdon, D. J. Chadderdon, J. E. Matthiesen, Y. Qiu, J. M. Carraher, J. P. Tessonnier, W. Li, *J. Am. Chem. Soc.* **2017**, *139*, 14120–14128.
[20] S. Jung, E. J. Biddinger, *ACS Sustain. Chem. Eng.* **2016**, *4*, 6500–6508.
[21] P. Chen, W. Zhang, J. Tan, Y. Yang, Y. Jia, Y. Tang, Q. Gao, *Catal. Sci. Technol.* **2022**, *12*, 4032–4039.
[22] R. Sander, *Atmos. Chem. Phys.* **2015**, *15*, 4399–4981.
[23] S. K. Green, J. Lee, H. J. Kim, G. A. Tompsett, W. B. Kim, G. W. Huber, *Green Chem.* **2013**, *15*, 1869–1879.
[24] J. A. Lopez-Ruiz, U. Sanyal, J. Egbert, O. Y. Gutiérrez, J. Holladay, *ACS Sustain. Chem. Eng.* **2018**, *6*, 16073–16085.
[25] A. M. Paolcaro, S. Palmas, S. Dernini, *Industrial & Engineering Chemistry Research* **1993**, *32*, 1315–1322.
[26] Y. Song, U. Sanyal, D. Pangotra, J. D. Holladay, D. M. Camaioni, O. Y. Gutiérrez, J. A. Lercher, *J. Catal.* **2018**, *359*, 68–75.
[27] U. Sanyal, S. F. Yuk, K. Koh, M. Lee, K. Stoerzinger, D. Zhang, L. C. Meyer, J. A. Lopez-Ruiz, A. Karkamkar, J. D. Holladay, D. M. Camaioni, M. Nguyen, V. Glezakou, R. Rousseau, O. Y. Gutiérrez, J. A. Lercher, *Angew. Chemie* **2021**, *133*, 294–300.
[28] K. Koh, U. Sanyal, M. Lee, G. Cheng, M. Song, A. Glezakou, Y. Liu, D. Li, R. Rousseau, O. Y. G. Ø, A. Karkamkar, M. Derewinski, J. A. Lercher, *Angewandte Chemie* **2020**, *59*, 1501–1505.
[29] N. Shan, M. K. Hanchett, B. Liu, *J. Phys. Chem. C* **2017**, *121*, 25768–25777.
[30] A. S. May, S. M. Watt, E. J. Biddinger, *React. Chem. Eng.* **2021**, *6*, 2075–2086.
[31] A. S. May, E. J. Biddinger, *ACS Catal.* **2020**, *10*, 3212–3221.
[32] S. Jung, E. J. Biddinger, *Energy Technol.* **2018**, *6*, 1370–1379.
[33] I. K. M. Yu, F. Deng, X. Chen, G. Cheng, Y. Liu, W. Zhang, J. A. Lercher, *Nat. Commun.* **2022**, *13*, 7154.
[34] S. Wang, V. Vorotnikov, D. G. Vlachos, *ACS Catal.* **2015**, *5*, 104–112.
[35] U. Sanyal, S. F. Yuk, K. Koh, M. Lee, K. Stoerzinger, D. Zhang, L. C. Meyer, J. A. Lopez-Ruiz, A. Karkamkar, J. D. Holladay, D. M. Camaioni, M. Nguyen, V. Glezakou, R. Rousseau, O. Y. Gutiérrez, J. A. Lercher, *Angew. Chemie* **2021**, *133*, 294–300.
[36] C. J. Bondue, M. T. M. Koper, *J. Am. Chem. Soc.* **2019**, *141*, 12071–12078.
[37] S. Chen, R. Wojcieszak, F. Dumeignil, E. Marceau, S. Royer, *Chem. Rev.* **2018**, *118*, 11023–11117.
[38] S. Sitthisa, D. E. Resasco, *Catal. Letters* **2011**, *141*, 784–791.
[39] J. Durst, C. Simon, F. Hasche, H. A. Gasteiger, *J. Electrochem. Soc.* **2014**, *162*, F190–F203.
[40] J. Durst, A. Siebel, C. Simon, F. Hasché, J. Herranz, H. A. Gasteiger, *Energy Environ. Sci.* **2014**, *7*, 2255–2260.
[41] A. Zalineeva, S. Baranton, C. Coutanceau, G. Jerkiewicz, *Langmuir* **2015**, *31*, 1605–1609.
[42] T. Shinagawa, A. T. Garcia-Esparza, K. Takanabe, *Sci. Rep.* **2015**, *5*, 1–21.
[43] J. S. Zeng, A. P. Willard, K. Manthiram, *Nat. Commun.* **2021**, *12*, 1–10.
[44] R. Sundararaman, D. Vigil-fowler, K. Schwarz, *Chem. Rev.* **2022**, *12*, 10651–10674, https://doi.org/10.1021/acs.chemrev.1c00800.
[45] A. Holewinski, S. Linic, *J. Electrochem. Soc.* **2012**, *159*, H864–H870.
[46] M. Łukaszewski, A. Czerwiński, *J. Solid State Electrochem.* **2011**, *15*, 2489–2522.
[47] A. Rose, S. Maniguet, R. J. Mathew, C. Slater, J. Yao, A. E. Russell, *Phys. Chem. Chem. Phys.* **2003**, *5*, 3220–3225.
[48] A. Viola, R. Chattot, V. Martin, G. Tsirlina, J. Nelayah, J. Drnec, F. Maillard, *J. Phys. Chem. C* **2023**, *127*, 17761–17769.
[49] E. Pizzutilo, S. Geiger, S. J. Freakley, A. Mingers, S. Cherevko, G. J. Hutchings, K. J. J. Mayrhofer, *Electrochim. Acta* **2017**, *229*, 467–477.
[50] R. Chattot, I. Martens, M. Mirolo, M. Ronovsky, F. Russello, H. Isern, G. Braesch, E. Hornberger, P. Strasser, E. Sibert, M. Chatenet, V. Honkimäki, J. Drnec, *J. Am. Chem. Soc.* **2021**, *143*, 17068–17078.
[51] S. Liu, N. Govindarajan, K. Chan, *ACS Catal.* **2022**, *12*, 12902-12910, https://doi.org/10.1021/acscatal.2c03822.
[52] B. Liu, L. Cheng, L. Curtiss, J. Greeley, *Surf. Sci.* **2014**, *622*, 51–59.
[53] N. Hodnik, C. Baldizzone, S. Cherevko, A. Zeradjanin, K. J. J. Mayrhofer, *Electrocatalysis* **2015**, *6*, 237–241.
[54] G. Li, P. Y. A. Chuang, *Appl. Catal. B Environ.* **2018**, *239*, 425–432.
[55] J. Xu, P. Wang, R. Yu, Z. Zheng, S. Shoaib Ahmad Shah, C. Chen, *Mater. Lett.* **2020**, *260*, 126950.
[56] I. A. Pasti, N. M. Gavrilov, S. V. Mentus, *Int. J. Electrochem. Sci.* **2012**, *7*, 11076–11090.
[57] A. M. Patel, S. Vijay, G. Kastlunger, J. K. Nørskov, K. Chan, *J. Phys. Chem. Lett.* **2021**, *12*, 5193–5200.
[58] G. Li, B. Wang, D. E. Resasco, *ACS Catal.* **2020**, *10*, 1294–1309.
[59] M. H. Ho, R. Rousseau, J. A. S. Roberts, E. S. Wiedner, M. Dupuis, D. L. Dubois, R. M. Bullock, S. Raugei, *ACS Catal.* **2015**, *5*, 5436–5452.
[60] S. Hammes-Schiffer, *J. Am. Chem. Soc.* **2015**, *137*, 8860–8871.
[61] J. Han, F. M. Tao, *J. Phys. Chem. A* **2006**, *110*, 257–263.
[62] B. Kumar, J. P. Brian, V. Atla, S. Kumari, K. A. Bertram, R. T. White, J. M. Spurgeon, *ACS Catal.* **2016**, *6*, 4739–4745.
[63] J. Yano, S. Yamasaki, *J. Appl. Electrochem.* **2008**, *38*, 1721–1726.
[64] R. Shiratsuchi, Y. Aikoh, G. Nogami, *J. Electrochem. Soc.* **1993**, *140*, 3479–3482.
[65] J. Yano, T. Morita, K. Shimano, Y. Nagami, S. Yamasaki, *J. Solid State Electrochem.* **2007**, *11*, 554–557.
[66] K. W. Kimura, K. E. Fritz, J. Kim, J. Suntivich, H. D. Abruña, T. Hanrath, *ChemSusChem* **2018**, *11*, 1781–1786.
[67] S. Ishimaru, R. Shiratsuchi, G. Nogami, *J. Electrochem. Soc.* **2000**, *147*, 1864–1867.
[68] C. Wattanakit, T. Yutthalekha, S. Asssavapanumat, V. Lapeyre, A. Kuhn, *Nat. Commun.* **2017**, *8*, 1–8.
[69] D. C. Cantu, A. B. Padmaperuma, M. T. Nguyen, S. A. Akhade, Y. Yoon, Y. G. Wang, M. S. Lee, V. A. Glezakou, R. Rousseau, M. A. Lilga, *ACS Catal.* **2018**, *8*, 7645–7658.

Manuscript received: August 26, 2024
Revised manuscript received: October 04, 2024
Accepted manuscript online: October 21, 2024
Version of record online: November 06, 2024